e-issn. 2798-5245

Mechanical Engineering for Society and Industry

Published by:
Universitas Muhammadiyah Magelang

unimma
Universitas Muhammadiyah Magelang

Mechanical Engineering for Society and Industry

An important discussion medium for academia, society, and industry

| E-ISSN: 2798-5245 | Scopus Indexed | Sinta 1 |

Mechanical Engineering for Society and Industry (MESI) is an international peer-reviewed open-access journal that publishes high-quality research and innovation in mechanical engineering and related disciplines. The journal covers a broad range of topics, including mechanics, energy systems, materials engineering, manufacturing... [Read more..]

Principal Editor >> Editorial board

Prof. Dr. Ir. Muji Setiyo, M.T.
Universitas Muhammadiyah Magelang, Indonesia
Academic profile:

33 days	118 days	23%
Submission to First Decision	Submission to Accept	Acceptance Rate (Last Year)

Current Issue

Vol. 6 No. 1 (February 2026) **View All Issues →**

Editorial

Indonesian engineers, the free nutritious meal program (MBG) needs you!

Muji Setiyo

Vol. 6 No. 1 (February 2026) | 1-8

Articles

Effect of forging pressure and rotational speed on the quality of rotary friction welding of Al 6063 and copper joints

Yeni Muriani Zulaida, Muhammad Anis, Mahfudz Al Huda, Kirman, Hermawan Agus Suhartono

Vol. 6 No. 1 (February 2026) | 9-20

Articles

The role of aromatic rings, heterocyclic rings, and hydroxyl groups in increasing hydrogen production using activated carbon-based photocatalysts

Fitria Indra Septi, Willy Satrio Nugroho, Purnami, Dionysius Joseph Djoko Herry Santjojo, I Nyoman Gede Wardana

Vol. 6 No. 1 (February 2026) | 21-39

Articles

Energy, exergy, and economic (3E) of a single slope solar still by integrating hollow circular fins and soybean wax as a thermal energy storage system

Irfan Santosa, Muhamad Dwi Septiyanto, Solikin Andriyanto, Eko Prasetya Budiana, Syamsul Hadi

Vol. 6 No. 1 (February 2026) | 40-64

Articles

SCADA-driven variable similarity-based model for fault detection and predictive maintenance in photovoltaic systems

Achmad Widodo, Toni Prahasto, Agussalim Syamsuddin, Andrew Cahyo Adhi, Amie Kusumawardhani

Vol. 6 No. 1 (February 2026) | 65-80

Articles

Identifying and evaluating sustainability risks in circular business models: Empirical insights from the heavy equipment manufacturing industry

Yudi Syahrullah, Udisubakti Ciptomulyono, Ratna Sari Dewi

Vol. 6 No. 1 (February 2026) | 81-100

Articles

Dual pillars of agro-energy transition: Irrigation efficiency and corn waste pyrolysis-fermentation for sustainable ethanol production in Papua lowlands

Suyatno, Helen Riupassa, Marthina Mini, Rolling S. Gaspersz, Hendry Y. Nanlohy

Vol. 6 No. 1 (February 2026) | 101-113

Articles

Corrosion behavior of ST37 low carbon steel welded joints in acidic and basic environments: implications for structural durability

Andika Wisnujati, Mudjijana, Syamsul Ma'arif, Satriardi, Hojjat Bagban

Vol. 6 No. 1 (February 2026) | 114-127

Articles

Improving the thermal efficiency of fin-tube heat exchangers by optimizing geometric parameters of curved rectangular winglet vortex generators

Articles

Effect of tool rotation direction, pin overlap, and pin shape on material flow in one-step double-acting friction stir welding of stainless steel: A Modeling study

Eko Prasetya Budiana, Rian Firmanda, Essam R. I. Mahmoud, Triyono

Vol. 6 No. 1 (February 2026) | 146-164

Articles

Perspective and modeling requirement on household solid waste management

Aswan Munang, Hari Purnomo, Winda Nur Cahyo, Imam Djati Widodo

Vol. 6 No. 1 (February 2026) | 165-179

Articles

Innovative integration of solar energy and pyrolysis technology in fish smoking for improved liquid smoke yield and quality

Risse Entikaria Rachmanita, Haning Hasbiyati, Refa Firgiyanto, Mohamad Anggis Safii Wijaya, Isrolana, Ellya Dwi Lestari, Bayu Rudiyanto

Vol. 6 No. 1 (February 2026) | 180-193

Articles

Stochastic analysis of time series temperature in battery cooling with ejector bubble generator

IGNB Catrawedarma, Sefri Ton, Anggra Fiveriati, Achilleus Hermawan Astyanto

Vol. 6 No. 1 (February 2026) | 194-210

Articles

Optimization of biodiesel synthesis process from nyamplung (calophyllum inophyllum) oil using thermal air sparging method

Nasrul Ilminnafik, Dani Hari Tunggal Prasetiyo, Welayaturromadhona, Audiananti Meganandi Kartini, Bekti Palupi, Suyitno

Vol. 6 No. 1 (February 2026) | 211-229

Articles

The influence of coffee ground waste on the thermal and mechanical characteristics of polymer-based 3D printing filament materials

Sally Cahyati, Rudi Krusdianto, Daisman Purnomo Bayyu Aji, Januar Parlaungan Siregar, Joddy Arya Laskmono

Vol. 6 No. 1 (February 2026) | 230-239

Articles

Flash joule heating synthesis of porous graphene oxide from banana leaf waste for high-performance supercapacitor electrodes

Ikhwanul Qiram, Dewi Sartika, Wisnu Kuncoro, Willy Satrio Nugroho, Abdul Mudjib Sulaiman Wahid

Vol. 6 No. 1 (February 2026) | 240-254

Articles

Spring-back effect on double arrowhead auxetic structures for EV battery compartment protectors

Asep Indra Komara, Indrawanto, Rachman Setiawan, Bagus Budiwantoro, Dedy Ariefijanto

Vol. 6 No. 1 (February 2026) | 255-270

Articles

Comparative performance of tapioca-starch bioplastics reinforced with pandan and grass jelly extracts

Putu Hadi Setyarini, Abdul Mujib Sulaiman Wahid, Madza Awwalul 'Atieq, Muhammad Rif'at Zulkarnain, Sisca Fajriani, Francisca Gayuh Utami Dewi, Dwi Hadi Sulistyarini, Ferry Bayu Setiawan

Vol. 6 No. 1 (February 2026) | 271-284

Articles

An experimental approach to evaluate the stability and thermal conductivity of SiO_2/oil as green nanolubricant

Anwar Ilmar Ramadhan, Tri Yuni Hendrawati, Kushendarsyah Saptaji, Efrizon Umar, Kukuh Haryadi

Vol. 6 No. 1 (February 2026) | 285-295

Corrigendum

Corrigendum to “The new modification of a solar still chamber with hollow glass: An experimental comparison between perpendicular and inline hollow glass configurations” [MESI Vol. 5, No. 2 (2025) pp 331-341]

Eko Prasetyo Budiana, Muhamad Dwi Septiyanto, Satria Auliansyah, Naufal Rizky Sayyid, Indri Yaningsih, Syamsul Hadi

Vol. 6 No. 1 (February 2026) | 296-297

Quick Links

Imprint Information

About the Journal

Guide for Author

Submit Your Manuscript

Announcements

View All

MESI Website Recovery and OJS Upgrade
2026-06-13

MESI has been accepted in Scopus
2023-09-12

Viewed | Downloaded

Energy, exergy, and economic (3E) of a single slope solar still by integrating hollow circular fins and soybean wax as a thermal energy storage system
Published: 63 Views

The stress corrosion cracking (SCC) susceptibility of the dissimilar ASTM A36 steels and 316L stainless steels welding in varied temperature of FeCl2
Published: 61 Views

Indonesian engineers, the free nutritious meal program (MBG) needs you!
Published: 55 Views

Stochastic analysis of time series temperature in battery cooling with ejector bubble generator
Published: 54 Views

The influence of coffee ground waste on the thermal and mechanical characteristics of polymer-based 3D printing filament materials
Published: 53 Views

Publisher: Universitas Muhammadiyah Magelang
Jl. Bambang Sugeng KM. 05 Mertoyudan, Magelang
Phone: (+62) 293 326945

e-ISSN: 2798-5245
Peer-Reviewed & Open-Access Journal

 Platform & workflow by Open Journal Systems (OJS)

Type of contribution:
Editorial
▶ Research Paper
Case Study
Review Paper
Scientific Data
Report of Tech. Application

mesi
e-issn. 2798-5245

Mechanical Engineering for Society and Industry
Vol. 6, No. 1 (2026) pp 194-210
https://doi.org/10.31603/mesi.15257

Stochastic analysis of time series temperature in battery cooling with ejector bubble generator

IGNB Catrawedarma[1]*, Sefri Ton[2], Anggra Fiveriati[1], Achilleus Hermawan Astyanto[3]

[1] Department of Mechanical Engineering, Politeknik Negeri Banyuwangi, Banyuwangi 68461, **Indonesia**
[2] Department of Agribusiness, Politeknik Negeri Banyuwangi, Banyuwangi 68461, **Indonesia**
[3] Department of Mechanical Engineering, Universitas Sanata Dharma, Sleman 55281, **Indonesia**
✉ ignb.catrawedarma@poliwangi.ac.id

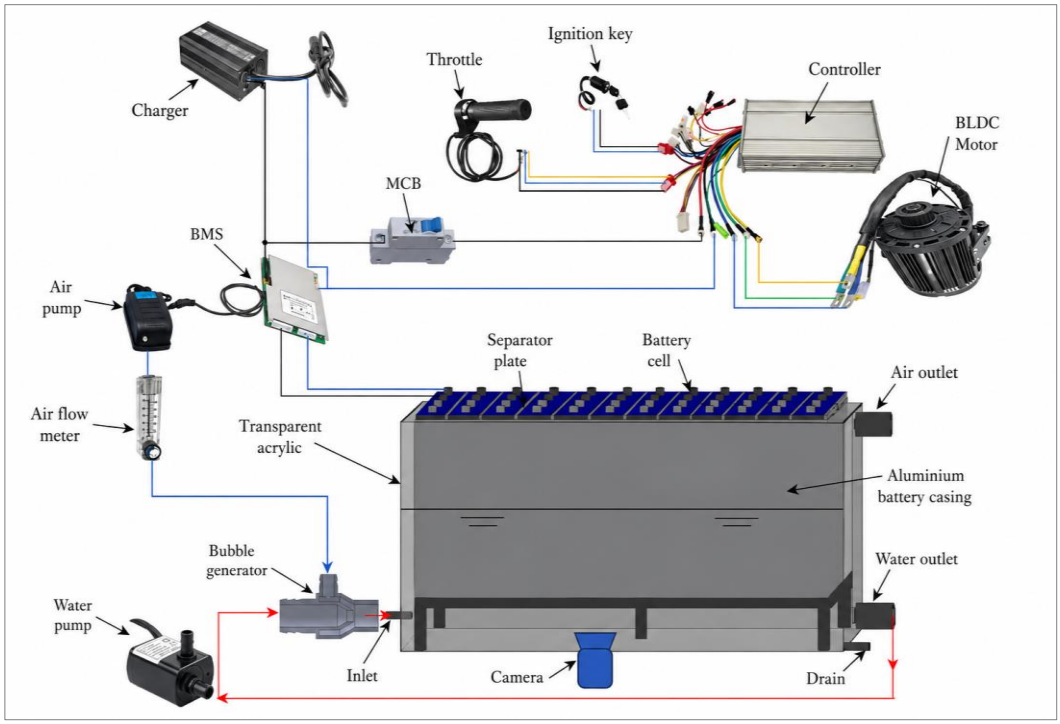

Highlights:

- Ejector bubbles enhanced cooling of LiFePO4 battery packs.
- Quiet air, circulating air, and bubble cooling modes were tested.
- Slug film, elongated slug film, and clustered bubbles were observed.
- At 1.5 lpm, Tmax and thermal resistance fell by 3.75% and 5.98%.
- Higher airflow reduced PDF kurtosis and sample entropy.

Article info
Submitted: 2025-11-06
Revised: 2026-04-12
Accepted: 2026-05-14

Publisher
Universitas Muhammadiyah Magelang

Abstract

This study identifies flow patterns in the cooling channels and analyzes temperature during $LiFePO_4$ battery cooling using an ejector bubble generator. The cooling fluids included quiet air, circulating air, and bubbles, with airflow rates ranging from 0.1 to 1.5 lpm. The temperature patterns were analyzed using probability density functions (PDFs), and Sample entropy—PDFs were quantified using mean, variance, skewness, and kurtosis. The results showed the formation of a slug film, an elongated slug film, and clustered bubbles on the bottom wall of the battery pack. There was a 3.75% and 5.98% decrease in the maximum temperature and thermal resistance, respectively, at an airflow rate of Qa = 1.5 lpm. The farther the thermocouple is from the bubble-generator nozzle and the greater the supplied airflow, the lower the PDF's kurtosis. The greater the airflow, the lower the entropy.

Keywords: Slug film; Thermal resistance; Chaotic analysis

1. Introduction

Rising oil prices, increasing demand to reduce the transportation sector's carbon footprint, and significant concerns about environmental pollution have motivated the development of electric vehicle technology [1], [2]. Electric vehicles offer high energy efficiency, diversification of energy resources, equitable distribution of power system loads, minimal exhaust emissions, and sufficient operation [3]. However, several factors still hinder the widespread commercialization of electric vehicles, such as a lack of reliability for long-distance travel and a relatively short vehicle lifespan, especially related to battery longevity [4]. Several factors affect battery performance, but the main factor is its susceptibility to thermal effects [1], [2], [5], [6]. Conventional Li-ion electric vehicle battery packs operate optimally between 15 °C and 35 °C. Because batteries are electrochemical systems, operating them below optimal temperature can reduce capacity and increase internal resistance [7]. Conversely, higher temperatures can cause premature aging of the battery, thermal runaway, decreased battery capacity, and even fires [7], [8], [9]. Therefore, several battery-cooling systems have been developed and tested to maintain the battery's operating temperature within the optimal range [10], [11], [12], [13].

The most basic types of battery cooling systems are air cooling [14], [15], liquid cooling [16], [17], [18], [19], [20], fin cooling [21], [22], solid-liquid phase change material (PCM) [5], [6], [7], [16], [21], heat pipe cooling [5], [8], [23], thermos-electric cooling [2], [24], [25], and combines two or more of these cooling systems [3], [16], [21], [24], [26], [27], [28]. All cooling methods have advantages and disadvantages in terms of manufacturing, maintenance, cost, and thermal performance. Air cooling is a conventional method that is simple to manufacture and maintain, making it more economical. Still, it has challenges in increasing heat dissipation capacity and accelerating temperature reduction. Its heat dissipation performance is not good enough when applied to battery cooling because its thermal conductivity is low [29].

Liquid cooling, both direct and indirect, offers the potential for good thermal performance but requires additional external power to move water into the battery pack, making it more complex to manufacture and maintain and less economical [30]. Immersion cooling can reduce thermal runaway, has low thermal resistance, and is relatively easy to manufacture [18], [31], [32], [33], [34], [35]. However, immersion cooling is compatible only with certain working fluids and can increase flow energy losses when using high-viscosity fluids, ultimately making it less economical.

PCM cooling utilizes the latent heat capacity of materials undergoing phase change from solid to liquid to reduce the heat produced in batteries [5], [16]. This cooling method has drawbacks regarding low thermal conductivity, difficulty controlling phase changes, and high heat accumulation. Therefore, a combination with high-thermal-conductivity media, such as graphite sheets [23], paraffin-graphene [24], graphite [25], silica [26], copper and nickel foams [27], [28], is required. This combination only increases the battery's heat dissipation capacity and increases the heat accumulation in the PCM. Combining a PCM with a heat pipe is one alternative to reduce heat accumulation in the PCM.

Heat pipes transfer heat without moving components and are highly efficient because they combine water and air cooling. Their manufacturing costs are relatively high because they must be airtight, corrosion-resistant, and require high-precision manufacturing processes. Heat pipe performance is strongly influenced by gravity, and it is necessary to increase the thermal contact between the battery and the heat pipe to improve temperature distribution and heat dissipation capacity [5], [8], [23]. Thermoelectric cooling, which uses the Peltier effect for heat dissipation, provides optimal temperature control but has low thermal efficiency in battery cooling, so it needs to be combined with other cooling methods [2], [36], [37], [38]. In addition, this method is closely related to higher manufacturing costs.

Another cooling method that needs to be developed is injecting bubbles into the battery cooling channel. Bubble cooling has so far been applied only to heat exchangers [39], [40], [41]. There was an increase in the number of transfer units (NTU) by up to 12.4% due to air bubbles injected into the heat exchanger plate, while the effectiveness increased by up to 14.6%. On the other hand, the increase in entropy reached 4.1 W/K [39]. The effect of bubbles on the thermal performance of heat exchangers was studied, and the results showed that the maximum increases in NTU and effectiveness were 153% and 68%, respectively [40]. The thermal performance of the heat exchanger was improved by increasing the bubble size. The bubble injection technique played an essential role in increasing NTU and effectiveness by 59% and 18.6%, respectively, on the cold-water side of the heat exchanger [41].

Most applications of bubbles as coolants still focus on conventional heat transfer systems, such as heat exchangers or common fluid flow channels [39], [40], [41], [42]. The application of bubble-injection mechanisms in battery-cooling systems remains relatively limited. Unlike conventional heat transfer systems, battery cooling systems have several special requirements, including uniform temperature distribution across cells, limited space in the battery pack, and the need for energy-efficient cooling [43], [44]. Therefore, effective heat transfer enhancement mechanisms in conventional heat exchangers do not necessarily provide the same performance when applied to battery cooling systems.

Based on the aforementioned research gap, this study aims to experimentally investigate the application of an ejector-type bubble generator, as characterised by Catrawedarma *et al*. [45], in a battery cooling system. The main focus of this study is to evaluate how bubble formation affects the maximum battery temperature, the temperature distribution, and the system's thermal resistance. This study also conducts further analysis on statistical parameters to provide a quantitative rationale for the effect of chaotic flow on battery thermal performance. Thus, this study provides new insights into the potential of using a bubble-injection-based two-phase flow mechanism to improve the performance of a battery cooling system.

2. Apparatus, Methods, and Procedure

This research was conducted at the Mechanical Engineering Workshop of Politeknik Negeri Banyuwangi, where apparatuses were installed following the schematic in **Figure 1a**. The materials and tools used include a 2 mm thick aluminum plate as a battery pack wrapper so that the battery does not come into direct contact with the coolant, a 3 mm thick transparent acrylic plate for visualizing the bubble flow in the cooling channel, 24 units of prismatic $LiFePO_4$ batteries with nominal capacity of 30 Ah and a nominal voltage of 3.2 V connected in series, 1 unit of battery management system with 24 pins to regulate the distribution of electricity to all battery cells, water as a cooling medium, one unit of 2000W mid-driven BLDC electric motor as a load on the battery, a controller to control the electric current to the motor, a 2.4W DC5V water pump to circulate water, a 1.0 W air pump to circulate air, an ejector type bubble generator to form bubbles [45], [46], [47], a high-speed camera to record video of the bubble flow in the cooling channel, and a 50W LED lamp for increased illumination when recording videos. The measuring instruments used include water and air flow meters to measure the input water and air flow, 12 K-type thermocouples to measure the bottom wall temperature of the battery pack, and the input and output temperatures, with thermocouple placement as shown in **Figure 1b**.

The data collection phase begins by filling the cooling gap with water through the air outlet to a height of 8.0 cm. A Lutron BTM-4208SD data logger with a sampling rate of 1.0 data points every 3.0 seconds was turned on to record the temperature. The water and air pumps were turned on, and the water flow rate was set to 3.4 lpm using the air flow meter, and the air flow rate was set to 0.1 lpm. Five minutes after the system stabilized, a high-speed video recording was conducted. Next, the ignition key was turned on to start the electric motor at maximum speed. This process begins to load the battery by maintaining a discharge current of 24.6 amperes and keeping the water level in the cooling channel to ensure the system operates steadily. The motor was turned on for 1800 seconds, and the temperature was recorded for 10800 seconds to observe temperature changes at no load. Repeat the steps above for various airflow rates from 0.1 to 1.5 lpm by adjusting the airflow meter. For quiet-water research, the steps are the same as above, but the water and air pumps were not turned on. For research with circulating water, only the water pump was turned on, with the air pump off. The data processing stage involved visualizing the flow and image processing of the bubble flow video, analyzing the temperature distribution and thermal resistance. The temperature time series was processed to obtain statistical moments, the PDF, and the chaotic level, which were used to assess the bubble's ability to cool the battery.

To ensure reproducibility of the results, each experimental condition was repeated three times with the same operating parameters. The temperature values reported in the manuscript are the average of the experimental repetitions, with an average difference of 0.1 °C, indicating that the experimental system has good stability and repeatability. The thermal resistance uncertainty was calculated using the error propagation method, accounting for uncertainties in temperature and heat power measurements. The accuracy of the thermocouple and input power is about 0.4% and 3%, so that the uncertainty in the calculation of thermal resistance is ±0.005467 °C/W.

To strengthen the validity of the experimental results, temperature and thermal resistance data were statistically analyzed by calculating means, standard deviations, and confidence intervals. The main results were reported with 95% confidence intervals; this analysis also helps ensure that the performance differences between conditions with and without bubble injection are outside normal experimental variation, thereby confirming the observed improvements are statistically significant.

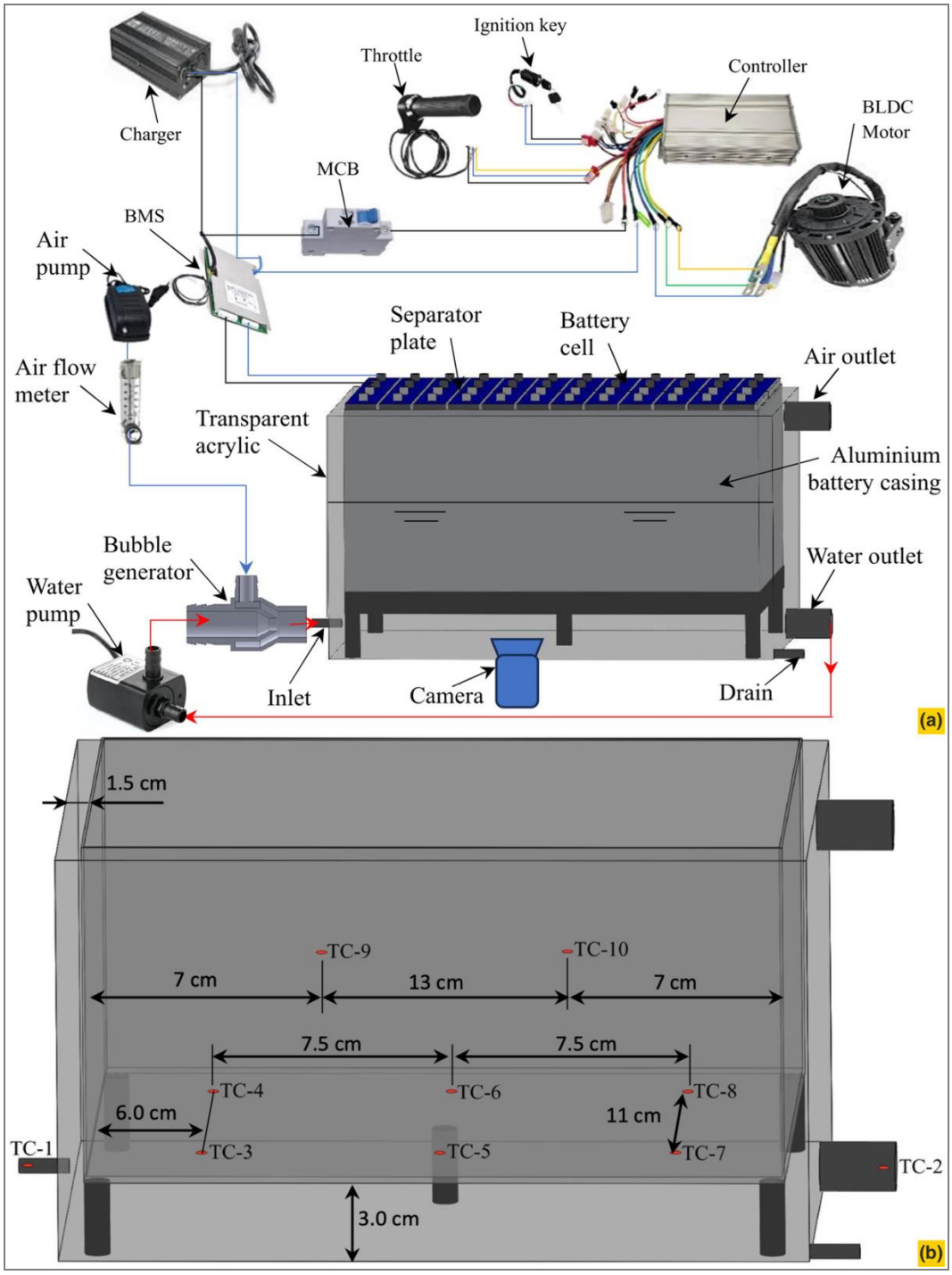

Figure 1. (a) Schematic diagram of battery cooling by bubble generator; (b) Thermocouple position

3. Results and Discussion

3.1. Bubble Flow Structure

Figure 2 illustrates the bubble flow changes from the bubble generator and the flow in the cooling water under the battery casing. Overall, elongated slug films, slug films, and clustered bubble films are attached to the bottom of the battery casing. Clustered bubbles are a group of bubbles gathered in a particular area, slug films are layers that are longer than bubbles due to the

merging of several bubbles, and elongated slug films are layers that are longer than slugs due to the merging of several slug films. The differences among these three films are shown in **Figure 2a**. When bubbles continue to be injected, several clustered bubbles merge into an unstable slug film, which is characterized by an unstable/wavy slug surface. In this condition, elongated slug films still form near the bubble generator nozzle as shown in **Figure 2b**. Bubble merging continues to occur due to the continuous supply of bubbles from the bubble generator, so that the unstable slug surface will become more stable and form a slug film as in **Figure 2c**. The bubble supply continues to be provided by the bubble generator, and bubble merging continues to occur, especially in areas further from the nozzle, which ultimately results in several slug films merging with other bubbles and slug films to form an elongated slug film, as in **Figure 2d**.

Figure 2e shows the onset of surface instability of the elongated slug due to the merging of several slugs and bubbles, which causes the bubble volume to increase and is followed by an increase in buoyancy so that the elongated slug part, which has high buoyancy, will begin to detach and start flowing upwards as in **Figure 2f**. The upward bubble will get bigger, followed by the slug film and other bubbles dragged to form a large bubble, as in **Figure 2g**. The large bubble rises and

Figure 2. Flow characteristic of bubble in the battery cooling mechanism: (a) Frame-1, t=0s; (b) Frame-66, t=1.94s; (c) Frame-78, t=2.29s; (d) Frame-103, t=3.03s; (e) Frame-154, t=4.53s; (f) Frame-155, t=4.56s; (g) Frame-159, t=4.68s; (h) Frame-162, t=4.76s; (i) Frame-164, t=4.82s; (j) Frame-172, t=5.06s

detaches from the bottom wall of the battery casing, forming a clustered bubble again, as in **Figure 2h**. The large bubble continues to rise until the buoyancy force is no longer sufficient to overcome the hydrodynamic forces of the surrounding water. The large bubble's velocity will decrease. However, the velocity of the water dragged around it remains high and finally penetrates the large bubble, forming a spike that drags the elongated slug near the nozzle, as in **Figure 2i**. When water continues to penetrate, the large bubble will break into small bubbles as in **Figure 2j**. In this system, the larger-diameter bubble regime provides greater heat transfer because buoyancy and hydrodynamic forces are stronger, disrupting the slug layer that forms on the bottom wall of the battery casing. The larger the bubble diameter, the faster the slug layer detaches from the wall, thus increasing heat transfer.

3.2. Time Series Temperature

Figure 3a shows the temperature changes of the motor wall (TC-11) and the bottom wall of the battery in the area closest to the bubble generator nozzle (TC-3 and TC-4), compared to the water temperature at the inlet (TC-1) and outlet (TC-2). In general, the trend in all graphs is an increase in temperature to a maximum, followed by a decrease. The temperature of the motor wall (TC-11) increases significantly when the motor is started until 1800s when it is turned off, as in area (i). The area is also called the heating or battery discharge area. Furthermore, in area (ii), there is a cooling process or a decrease in temperature of the motor and the bottom wall of the battery. However, the temperature at TC-1 and TC-2 tends to be constant, as in area (iii), which is called the steady cooling area. The area is the peak point for TC-1 and TC-2. Furthermore, in area (iv), all temperatures experience a decrease. It indicates that cooling stability has been achieved.

The increase in battery temperature (TC-3 and TC-4) is also not as drastic as the motor wall temperature (TC-11). The temperature of TC-3 is not significantly different from the temperature of TC-4 because it is parallel to the bubble generator nozzle. However, both temperatures are higher than the temperatures of TC-1 and TC-2. The temperature at the outlet side (TC-2) is greater than that at the inlet side (TC-1) because, as in flows, the water from the inlet side absorbs heat from the battery cell, increasing the temperature of the cooling water at the outlet side. Heat from the bottom wall of the battery cell is transferred by conduction to the aluminum bottom surface of the battery casing. The heat from the aluminum bottom wall is transferred to the water, and bubbles rise through it by convection. The cooling water flows to the outlet side, then returns to the bubble generator via the water pump. The maximum temperature of the battery wall is 31.0 °C, and the maximum temperature from the outlet side is 29.6 °C. After reaching the maximum point, the battery temperature decreases gradually, unlike the exponential decrease in the walls

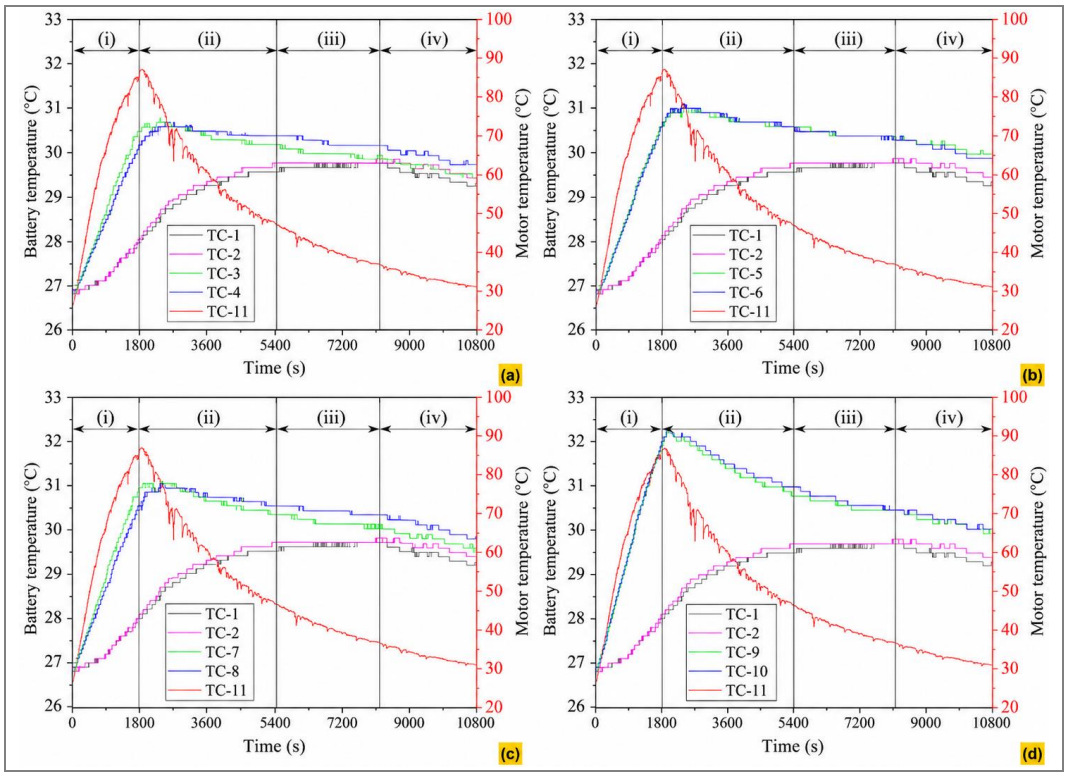

Figure 3. Temperature distribution at Qa = 0.1 lpm: (a) Time series temperature at front region (TC-3 and TC-4); (b) Time series temperature at middle region (TC-5 and TC-6); (c) Time series temperature at rear region (TC-7 and TC-8); (d) Time series temperature at center region (TC-9 and TC-10)

of an electric motor. It is caused by the electric motor being in direct contact with ambient air; chemical reactions in the battery cells also contribute.

Figure 3b compares the temperatures in the center of the bottom wall of the battery in TC-5 and TC-6. Both temperatures are above the inlet (TC-1) and outlet (TC-2) temperatures of the cooling water, with a maximum temperature of 31.2 °C. The temperature is slightly higher than in the area closer to the nozzle in TC-3 and TC-4, shown in **Figure 3a**. **Figure 3c** shows the temperature changes in TC-7 and TC-8 compared to the motor temperature (TC-11), input temperature (TC-1), and output temperature (TC-2). The maximum temperature in TC-7 and TC-8 is 31.3 °C; it is the highest because it is the area closest to the cooling water outlet. **Figure 3d** is an interpretation of the temperature in the middle of the battery wall of TC-9 and TC-10. The thermocouple is located in the midpoint of the width and height of the battery cell pack. With a maximum temperature of 32.3 °C, the temperature is higher than that on the bottom wall of the battery. It indicates that the middle part of the battery is hotter than the top and bottom.

Figure 4a and **Figure 4b** show the temperature changes from upstream (the area closest to the inlet), middle, and downstream (the area furthest from the inlet). The temperature closest to the inlet is lower. The further from the inlet, the higher the temperature. It is caused by an outlet temperature higher than the inlet temperature, resulting in lower heat absorption when the cooling water exits the outlet. In addition, an air film on the bottom wall of the battery can raise temperatures by increasing thermal resistance. It is known that the temperature rises by 0.6% from upstream to the middle, increases by 0.3% from the middle to downstream, and increases by 3.1% from downstream to the middle wall of the battery.

The motor temperature in **Figure 3** and **Figure 4** is used to show the system's overall thermal response during operation. The trendline graph shows that the motor temperature fluctuates after the motor is turned off, in contrast to the battery temperature, which does not fluctuate and tends to decrease slowly. These two temperatures are not directly related and do not influence each other because they have different mechanisms for temperature change. Battery temperature is strongly influenced by the C-rate, the battery's internal resistance, and the electrochemical processes that occur during charging and discharging [27]. Meanwhile, motor temperature is influenced by mechanical load, motor efficiency, electrical losses and the motor's cooling system. However, an indirect relationship between battery and motor temperatures occurs due to system loading. As the load increases, the C-rate increases, ultimately raising the battery temperature due to resistive losses. Under the same conditions, the motor works harder, generating more heat. The C-rate is a parameter that determines the amount of current flowing through the battery and affects internal heat generation [27].

Figure 5 shows the effect of bubbles injected into the cooling gap on the temperature distribution. It is known that the lower the air flow rate, the higher the maximum temperature of the battery wall. It is caused by the production of fewer, smaller bubbles, so that it takes longer to form an elongated slug film, and the longer this film sticks to the bottom wall of the battery pack. The phenomenon increases thermal resistance and prevents heat absorption by the coolant because the elongated slug film has a surface tension greater than the hydrodynamic force of water, thereby maintaining its shape and position. The elongated slug film will break and flow upwards if more bubbles come out of the nozzle, so that bubble merger occurs and the bubble volume increases, which implies a greater buoyancy force to move upwards and detach from the bottom wall of the battery packing [48], [49], [50]. The analysis is in accordance with the research of Hasan *et al*. [40]. Increasing the bubble size can improve a heat exchanger's thermal performance.

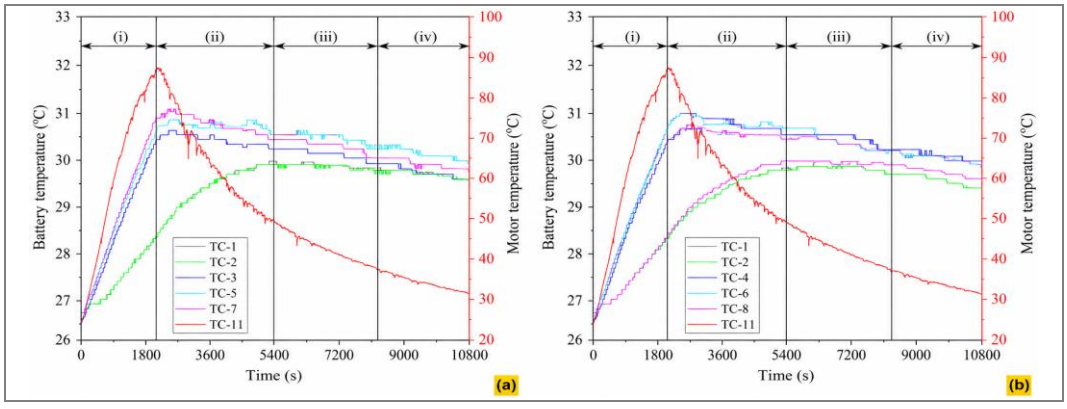

Figure 4. Temperature distribution at Qa = 0.5 lpm: (a) Time series temperature at left region (TC-3, TC-5, and TC-7); (b) Time series temperature at right region (TC-4, TC-6, and TC-8)

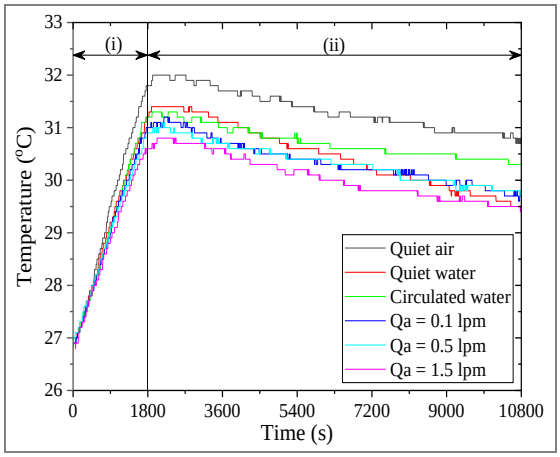

Figure 5. Temperature distribution at TC-7 for various of air flow rate

When comparing the quiet and circulating fluid, it is known that the circulating water has a slightly lower maximum temperature due to heat transfer by forced convection and advection. Also, water movement increases heat absorption. The maximum temperatures for quiet air, quiet water, circulated water, Qa = 0.1 lpm, Qa = 0.5 lpm, and Qa = 1.5 lpm, are 32 °C, 31.4 °C, 31.3 °C, 31.2 °C, 31.1 °C, and 30.8 °C, respectively. A maximum temperature decrease of 3.75% between the quiet air cooling fluid and the bubble cooler with an air flow rate of Qa = 1.5 lpm.

3.3. Thermal Performance

Thermal resistance is one indicator of a cooling system's thermal performance. Thermal resistance is the measure of a material's resistance to heat flow. In cooling systems involving convection heat transfer, thermal resistance includes convection thermal resistance due to heat transfer between the surface and the fluid, and advection thermal resistance due to heat transfer along the flow of the cooling fluid. The convection coefficient and surface area influence the convection thermal resistance, while advection thermal resistance is determined by the fluid's mass flow rate and heat capacity. The analysis only uses forced-moving cooling fluids, namely, circulated water and bubble injection, to understand convection and advection thermal resistance in depth.

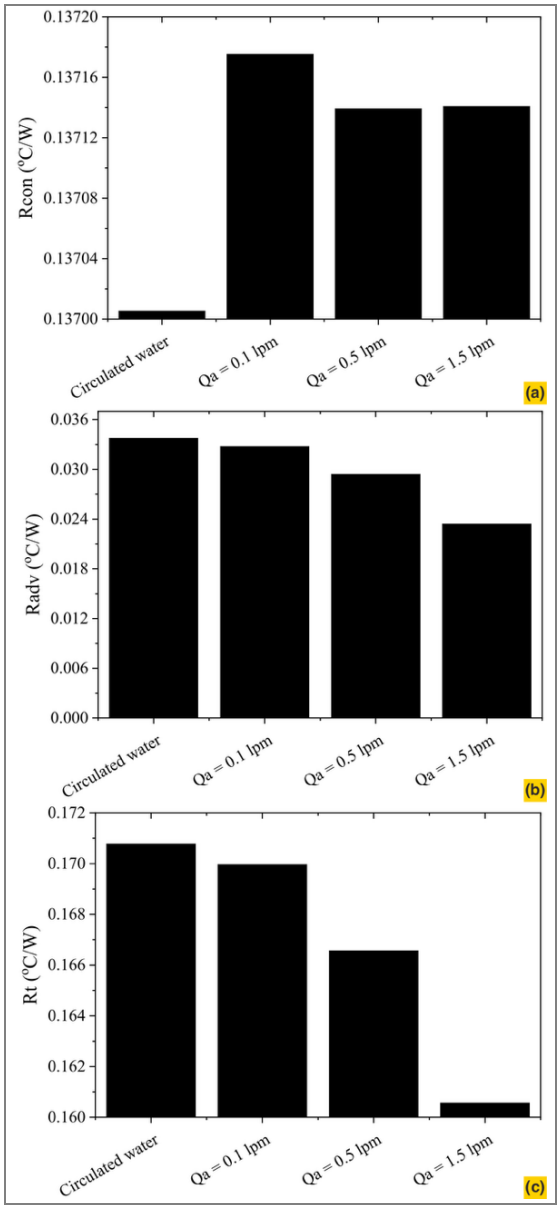

Figure 6. Thermal resistance: (a) Convection thermal resistance; (b) Advection thermal resistance; (c) Total thermal resistance

Figure 6a shows the convection thermal resistance for a moving coolant fluid. It is known that circulated water has the lowest convection thermal resistance of 0.13701 °C/W. Furthermore, the thermal resistance due to convection decreases as the input air flow rate increases. It is due to the increase in the convection coefficient as the water circulates. The convection coefficient is proportional to the Nusselt number, fluid velocity increases the Reynolds number, and the Nusselt number is a function of the Reynolds number and Prandtl. Therefore, fluid velocity significantly affects convection heat transfer.

Figure 6b shows that the advection thermal resistance decreases with increasing air flow rate. The cooling medium with water circulation has the highest advection thermal resistance. It is influenced by the increasing fluid mass flow rate when bubbles are injected. Due to the addition of bubbles, heat transfer occurs in the two-phase air-water flow as well as random movement of the cooling fluid due to collisions, mergers, and bursting of bubbles, thereby increasing the local velocity of the two-phase flow, which ultimately has implications for improving the mass flow rate of the cooling fluid.

Figure 6c shows the trend of total resistance, which is the sum of convection and advection resistance. It is known that the greater the air flow rate, the lower the total thermal resistance. The highest total thermal resistance is 0.17078 °C/W in the circulated water cooling fluid, and the lowest is 0.16057 °C/W, resulting in a decrease of 5.98%. Compared with **Figure 6a** and **Figure 6b**, the most influential factor in this cooling system is the advection thermal resistance, which is predominantly driven by changes in the cooling fluid's mass flow rate.

In this study, temperature distribution was analyzed by placing several temperature sensors at different points around the battery. The measurements showed that the cooling system maintained temperature differences between battery points within a relatively small range, thereby minimizing temperature gradients. The presence of two-phase flow with bubbles distributed within the fluid also helped improve fluid mixing, ultimately improving heat distribution within the system. Additionally, the fluid flow rate is set at a specific value to achieve a balance between increased heat transfer and pump energy consumption. The use of two-phase flow with bubble formation increases local turbulence and fluid mixing, thereby increasing the heat transfer coefficient without significantly increasing the flow rate, ultimately helping reduce pumping power requirements.

Experimental results show that bubbles in a two-phase flow enhance convection through microturbulence and increased interaction between the gas and liquid phases. It accelerates heat transfer from the battery surface to the coolant, thereby improving the system's overall thermal performance. Overall, the study's results indicate that the approach improves heat transfer and maintains uniform battery temperature, while keeping the pumping power requirement at an efficient level. These three aspects indicate that the studied system has the potential to be applied to practical battery thermal management systems, especially in systems with high cooling requirements, such as electric vehicles or energy storage systems.

Although the maximum temperature increase of 3.75% and the thermal resistance decrease of 5.98% appear relatively small, these values are still within the range of improvements often reported in optimization studies of cooling systems that are already close to optimal conditions [51]. This result is in accordance with that reported by Jauhari *et al*. [42], with a decrease of 6.1% from the battery without cooling to the hybrid paraffin oil-fan cooler. In battery applications, particularly in electric vehicles or energy storage systems, even a few degrees of temperature reduction can have a significant impact on battery life, performance stability, and operational safety [52]. Lower thermal resistance indicates that heat can be dissipated more effectively from the battery to the cooling medium. Therefore, small improvements at the laboratory level can yield greater benefits when applied to battery systems with larger cell counts, where heat accumulation becomes more significant [51].

The two-phase flow concept used in this study is theoretically applicable to larger systems because the heat transfer enhancement mechanism stems from bubble interactions and increased local turbulence, which are independent of system size. However, implementation at the module or battery-pack scale requires further optimization of fluid channel design, flow distribution, and bubble-formation control. The heat transfer increase in this system is achieved without a significant increase in fluid flow rate, resulting in relatively little additional pumping power. It is one of the advantages of this approach over performance improvements that rely solely on increasing fluid flow.

This research focuses primarily on demonstrating that a two-phase flow mechanism with bubble formation can reduce the thermal resistance of a battery cooling system. The results show a consistent trend of increasing thermal performance, which can serve as a basis for developing a more efficient battery-cooling design in future research, especially through optimization of parameters such as bubble size, flow rate, and cooling channel geometry.

3.4. Statistical Moments

Statistical moments are used to identify temperature time series patterns for quantitative, objective analysis. The statistical moments used include the mean, variance, skewness, and kurtosis. **Figure 7a** shows the average temperature for all cooling media from quiet air, quiet water, circulating water, and bubble cooler with air flow rate from 0.1 lpm to 1.5 lpm at all thermocouple positions. Part (i) shows the temperature of the inlet (TC-1) and outlet (TC-2) positions, part (ii) shows the temperature of the battery wall closest to the bubble generator nozzle (TC-3 and TC-4), part (iii) is the middle part of the bottom battery wall (TC-5 and (TC-6), part (iv) is the part furthest from the bubble generator nozzle (TC-7 and TC-8) and closest to the outlet side (TC-2). The lowest

average temperature is at TC-2, which is the cooling fluid outlet. The average temperature of quiet air has the greatest value due to its lower thermal conductivity.

Bubble cooling with an air flow of 1.5 lpm could optimally reduce the battery wall's temperature. It is evident from its average temperature, which has the lowest value among other cooling media. For all thermocouples, TC-9 and TC-10 had the highest average temperature values. It is evidence that the temperature of the battery wall in the center is the highest, and then it is distributed to the outer parts, which are getting lower by conduction. The average temperature on the battery wall tends not to increase significantly from TC-3 to TC-6. Still, there is a decrease in TC-7 and TC-8; this occurs because the influence of bubbles that emerge from the ejector is carried to the area closest to the outlet, leading to random flow, which significantly contributes to the temperature decrease. The average temperature on TC-9 and TC-10 is very high, even though the thermocouples are closer to the top, which is in contact with the atmosphere. It shows that atmospheric air is not so dominant in reducing the temperature of the battery wall. Instead, the chemical reactions in the battery are the main factors influencing changes in the battery wall's temperature.

Figure 7b shows the temperature variance for each thermocouple position and coolant treatment. This variance indicates temperature amplitude fluctuations. The largest fluctuations occur at the inlet and outlet because the measured temperature is the fluid temperature, which fluctuates wildly as the fluid moves. It differs from the stationary coolant, where temperature amplitude fluctuations are very low. Temperature amplitude fluctuations on the battery wall did not differ significantly between TC-3 and TC-8. Amplitude fluctuations increased at TC-9 and TC-10 because the thermocouples are positioned above, close to, atmospheric air with fluctuating temperatures.

Figure 7c shows the skewness values for all coolant treatments at various thermocouple positions. The skewness value indicates the deviation of a distribution curve from its symmetrical shape. It can be seen that all skewness values are negative, indicating that the temperature distribution is concentrated above the average temperature. The trend in the graph shows that TC-1, TC-2, TC-9, and TC-10 have a higher skewness than the temperature at the bottom wall of the battery. It indicates that the temperature at the bottom wall of the battery is more concentrated at values above the average. In other words, temperatures above the average occur more frequently.

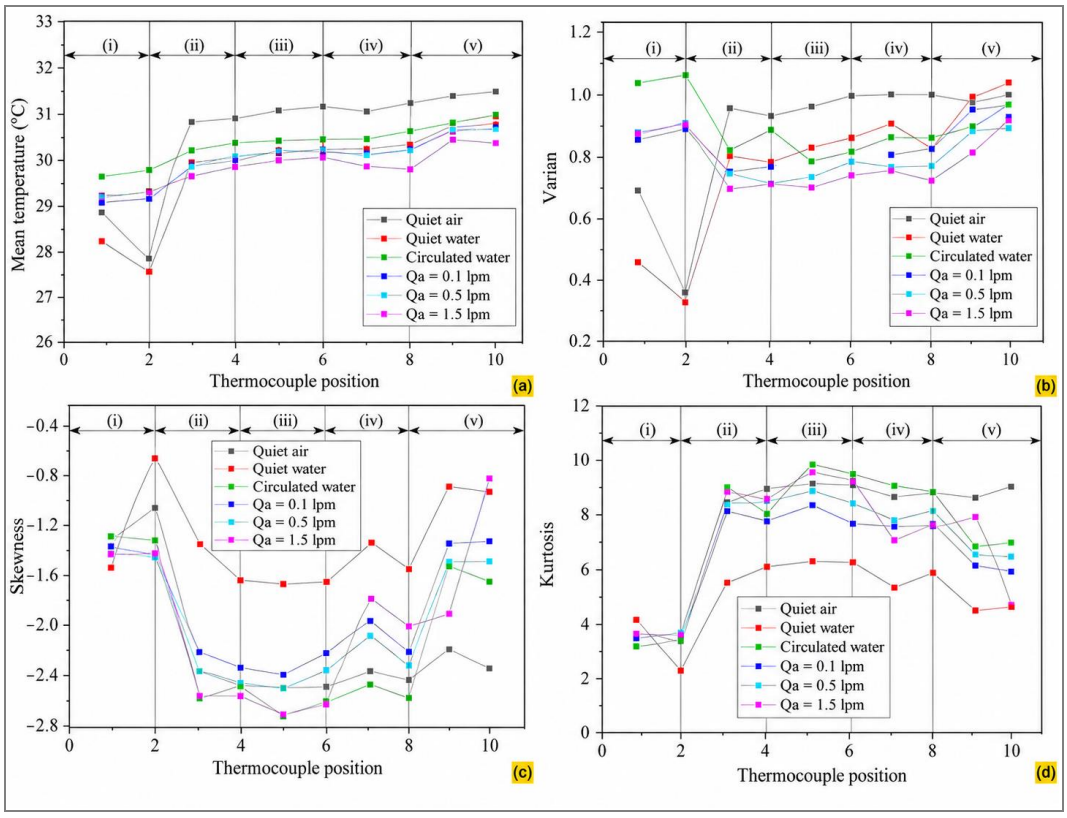

Figure 7.
Statistical parameter of temperature:
(a) Mean;
(b) Varian;
(c) Skewness;
(d) Kurtosis

Figure 7d displays the kurtosis values for each position and coolant treatment. Kurtosis is a measure of the flatness of the temperature distribution curve. A higher kurtosis indicates a sharper distribution curve, indicating a very low temperature distribution. It is evident in the temperature at the bottom of the battery, which has a higher kurtosis than at other thermocouple positions. It means that the temperature distribution on the bottom wall of the battery is minimal because it is determined by the battery's packaging material and the chemical reaction of the fluid inside the battery, which do not change over a wide range. Skewness and kurtosis are values that objectively characterize the temperature distributions shown in Figure 8 and Figure 9.

3.5. Probability Density Function

It is clearly seen in Figure 8 and Figure 9 that the temperature distributions at the inlet (TC-1) and outlet (TC-2) for all coolant treatments exhibit very high kurtosis; several temperature ranges have a very high frequency of occurrence. It is quite different from the temperature on the battery wall. No dominant temperature appears when the coolant is not moving (quiet air and quiet water). It is caused by insignificant temperature fluctuations and by natural heat transfer via convection, so the temperature decrease tends to be gradual. When the coolant is circulated (Qa = 0.1 to 0.5 lpm) to induce forced convection, the temperature distribution narrows, leading to several dominant temperatures and increased kurtosis. For the bottom wall temperature of the battery, TC-7 and TC-8 tend to exhibit PDFs with low kurtosis. It indicates a spread in the emergence of temperature due to the random flow pattern downstream of the ejector bubble generator. Entropy analysis is needed to see the random flow and temperature level more objectively, as in Figure 10.

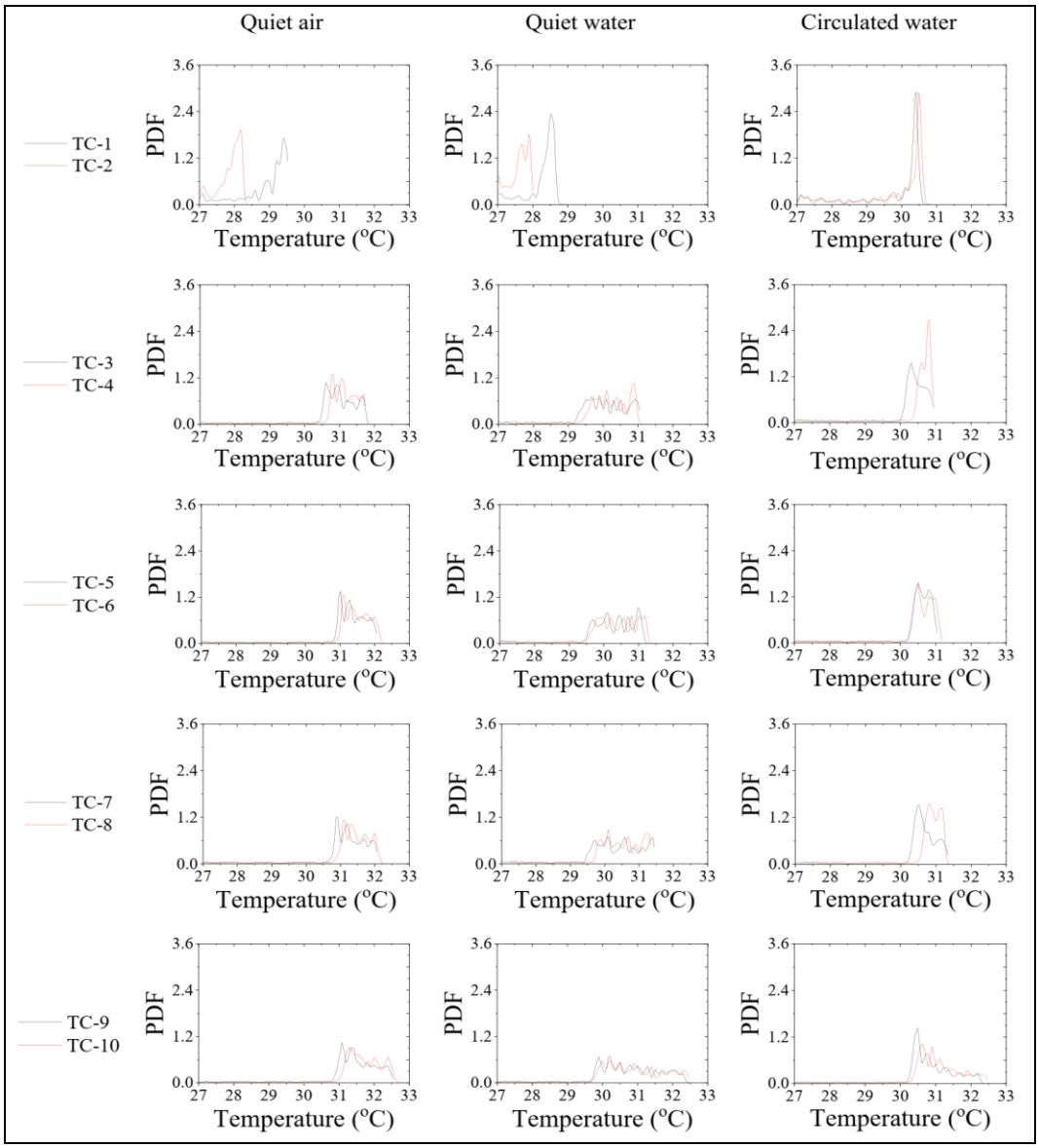

Figure 8. Probability density function for quiet air, quiet water, and circulated water

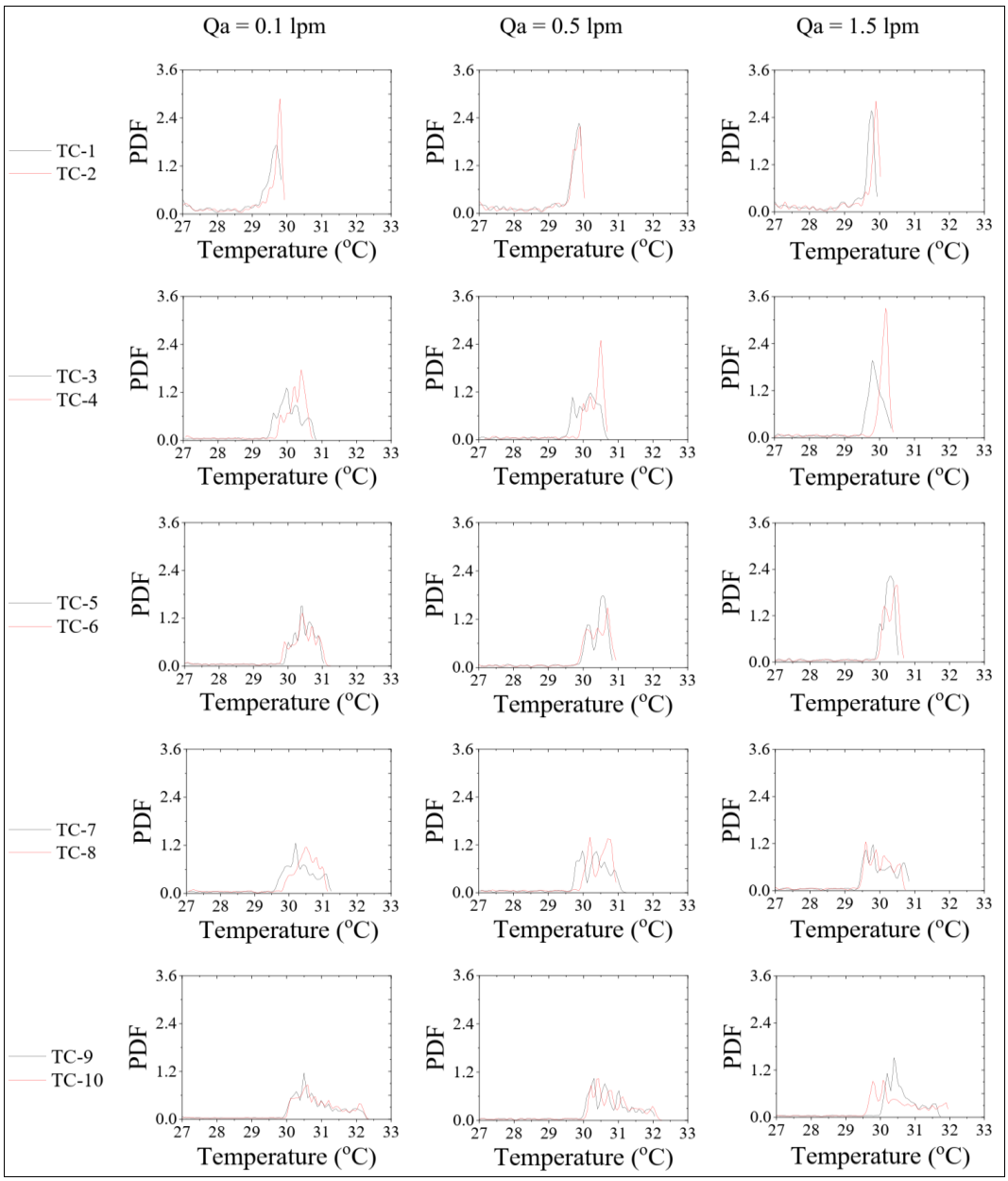

Figure 9. Probability density function for Qa = 0.1 lpm, 0.5 lpm, and 1.5 lpm

3.6. Chaotic Analysis

Chaotic systems are characterized by patterns that never repeat the same, or the level of regularity of the time series, which can be determined using several methods, such as the Kolmogorov-Smirnov [33], [34], Approximate entropy (AppEn) [53], and Sample entropy (SampEn) [54], [55]. The current study uses SampEn because it develops the AppEn and Kolmogorov methods. SampEn provides more accurate results than ApEn because it does not calculate self-matches (patterns that are compared with themselves) and is more stable for short datasets [54]. The SampEn calculation in this study uses parameters commonly used in physical time series analysis, such as the Embedding dimension (m), which is chosen to be 2, because this value is often used in experimental signal analysis to maintain a balance between sensitivity to data patterns and the need for sufficient data length [48], [56]. The tolerance (r) is set to 0.2 times the standard deviation of the data, a value widely recommended in the entropy analysis literature for physical and biomedical systems. This value allows the detection of similar patterns in the signal without being overly sensitive to measurement noise [57]. The selection of these parameters aims to ensure that the obtained entropy values reflect the real complexity of temperature dynamics.

Figure 10 shows the entropy of each temperature and cooling fluid position. A relatively large entropy occurs at the inlet and outlet for a stationary cooling fluid. It indicates that the temperature change pattern is irregular due to natural convection, which causes irregular movement of the cooling fluid. Circulating water tends to have the lowest entropy because the

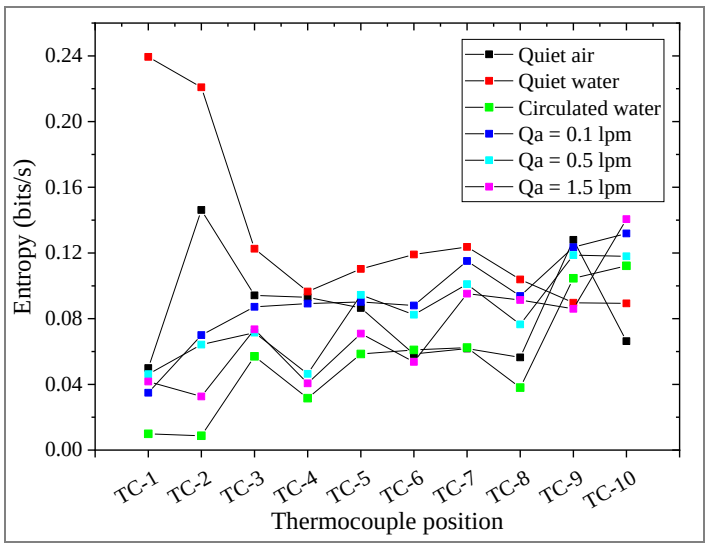

Figure 10. Kolmogorov entropy

fluid movement is regular, following the pump speed. The greater the supplied air flow, the lower the entropy. It is caused by the flow pattern of the supplied bubbles tending to move regularly due to the larger bubble diameter, so that the buoyancy force is greater, which causes the rising velocity to be greater, so that regular breakup of elongated bubbles occurs, which ultimately has an impact on regular temperature changes. The lower the air flow, the higher the entropy because the smaller the bubble diameter and the fewer bubbles produced, causing more random bubble movement due to the higher frequency of bubble merging and breaking [46], [47], as well as the longer time for elongated bubbles to break and detach from the bottom wall of the battery, which ultimately causes irregular temperature changes.

In the context of temperature dynamics in battery cooling systems, sample entropy is used to measure the complexity and irregularity of temperature fluctuations over time. Higher entropy values indicate a system experiencing more random and unstable temperature fluctuations, while lower entropy values indicate more orderly and stable thermal behavior. In this study, the decrease in entropy observed after bubble injection indicates that battery temperature fluctuations are better controlled. It indicates that the fluid-mixing mechanism induced by the bubbles can improve the stability of the heat transfer process. In other words, the decrease in entropy reflects a more stable thermal condition, which aligns with the experimental results showing a decrease in the maximum temperature and thermal resistance of the system.

Conventional thermal analysis of battery cooling systems typically focuses on macroscopic parameters, such as average and maximum temperatures and the heat transfer coefficient. This approach is effective for evaluating the system's overall performance, but often fails to capture the nonlinear and temporal dynamics of temperature fluctuations, particularly in two-phase flow systems. Stochastic characterization via statistical moments and sample entropy enables a more in-depth analysis of the temporal structure of the temperature signal. This method can identify changes in thermal dynamics patterns, such as the degree of instability of temperature fluctuations, changes in the complexity of thermal dynamics, and the system's response to two-phase flow disturbances. Thus, this approach provides additional insights into the system's thermal stability that are not readily apparent from average or maximum temperature parameters alone.

4. Conclusion

This study provides information on the potential of using bubble generators as a cooling medium in $LiFePO_4$ battery thermal management systems. It uses various cooling fluids, including air, water, and an air-water mixture. The flow patterns of the formed bubbles, the maximum temperature of the battery wall, thermal resistance, PDF, and chaotic system are analyzed to characterize the temperature time series. The PDF was quantified using statistical moments, including mean, variance, skewness, and kurtosis. The results can be summarized as follows:

- Slug film, elongated slug film, and clustered bubbles form on the bottom wall of the battery. The greater the injected airflow rate, the faster the elongated slug film detaches from the bottom wall, thereby improving thermal performance.
- Quiet air coolant has the highest maximum temperature compared to the others. The greater the air flow rate, the lower the maximum temperature. There is a 3.75% decrease in maximum temperature between quiet air and bubble coolant with an air flow rate of Qa = 1.5 lpm.
- The highest total thermal resistance is 0.17078 °C/W in the circulated water cooling fluid, and the lowest is 0.16057 °C/W in the cooling fluid with Qa = 1.5 lpm, resulting in a 5.98% decrease in thermal resistance.

- When the coolant is stationary (quiet air and quiet water), no dominant battery wall temperature is observed, resulting in a low-kurtosis PDF. The farther the battery wall thermocouple is from the bubble generator nozzle and the greater the air flow rate supplied, the lower the kurtosis of the PDF curve.
- Significant entropy occurs at the inlet and outlet of a stationary coolant fluid. Circulated water tends to have the lowest entropy. The greater the supplied air flow rate, the lower the entropy.

Acknowledgements

This research is one of the applications of bubble generators, which is part of the research project framework of the two-phase flow and heat transfer research group in the Department of Mechanical Engineering at Banyuwangi State Polytechnic. The authors thank Rizky Novan Wijaya, Deqi Pajar Pratama, and Moh. Yatim has helped design and manufacture research apparatus.

Authors' Declaration

Authors' contributions and responsibilities – IGNB Catrawedarma: Writing – original draft, Formal analysis, Data curation, Conceptualization. Sefri Ton: Validation, Project administration, Methodology, Investigation. AnggraFiveriati: Supervision, Resources, Funding acquisition. Achilleus Hermawan Astyanto: Writing – review & editing, Supervision, Conceptualization.

Funding – The authors also thank the Directorate of Research and Development, Ministry of Higher Education, Science, and Technology of the Republic of Indonesia, for financial support through the Regular Fundamental Research scheme, contract number 027/C3/DT.05.00/PL/2025.

Availability of data and materials – All data is available from the authors.

Competing interests – The authors declare no competing interests.

Additional information – No additional information from the authors.

References

[1] H. S. Hamut, I. Dincer, and G. F. Naterer, "Exergy analysis of a TMS (thermal management system) for range-extended EVs (electric vehicles)," *Energy*, vol. 46, no. 1, pp. 117–125, Oct. 2012, doi: 10.1016/j.energy.2011.12.041.

[2] F. S. Hwang *et al.*, "Review of battery thermal management systems in electric vehicles," *Renewable and Sustainable Energy Reviews*, vol. 192, no. December 2022, p. 114171, 2024, doi: 10.1016/j.rser.2023.114171.

[3] K. . Chau and Y. . Wong, "Overview of power management in hybrid electric vehicles," *Energy Conversion and Management*, vol. 43, no. 15, pp. 1953–1968, Oct. 2002, doi: 10.1016/S0196-8904(01)00148-0.

[4] G. Krishna, "Understanding and identifying barriers to electric vehicle adoption through thematic analysis," *Transportation Research Interdisciplinary Perspectives*, vol. 10, p. 100364, Jun. 2021, doi: 10.1016/j.trip.2021.100364.

[5] Q. Huang, X. Li, G. Zhang, J. Zhang, F. He, and Y. Li, "Experimental investigation of the thermal performance of heat pipe assisted phase change material for battery thermal management system," *Applied Thermal Engineering*, vol. 141, pp. 1092–1100, Aug. 2018, doi: 10.1016/j.applthermaleng.2018.06.048.

[6] M. Mahmud *et al.*, "Lithium-ion battery thermal management for electric vehicles using phase change material: A review," *Results in Engineering*, vol. 20, no. August, p. 101424, 2023, doi: 10.1016/j.rineng.2023.101424.

[7] L. Ianniciello, P. H. Biwolé, and P. Achard, "Electric vehicles batteries thermal management systems employing phase change materials," *Journal of Power Sources*, vol. 378, pp. 383–403, Feb. 2018, doi: 10.1016/j.jpowsour.2017.12.071.

[8] Y. Ye, Y. Shi, L. H. Saw, and A. A. O. Tay, "Performance assessment and optimization of a heat pipe thermal management system for fast charging lithium ion battery packs," *International Journal of Heat and Mass Transfer*, vol. 92, pp. 893–903, Jan. 2016, doi: 10.1016/j.ijheatmasstransfer.2015.09.052.

[9] D. M. Weragoda, G. Tian, Q. Cai, T. Zhang, K. Hing Lo, and Y. Gao, "Conceptualization of a novel battery thermal management system based on capillary-driven evaporative cooling," *Thermal Science and Engineering Progress*, vol. 47, p. 102320, Jan. 2024, doi: 10.1016/j.tsep.2023.102320.

[10] G. Shruti, P. B. Salunkhe, and B. S. Shenoy, "Recent progress on passive cooling strategies for Li-ion battery of electric vehicles," *Journal of Energy Storage*, vol. 156, p. 121550, Apr. 2026, doi: 10.1016/j.est.2026.121550.

[11] S. R. Patil, B. R. Lokavarapu, and H. K. Thaliyanveedu, "Optimization of battery cooling system used in electric vehicles," *Journal of Energy Storage*, vol. 58, p. 106299, Feb. 2023, doi: 10.1016/j.est.2022.106299.

[12] X. Wang, R. Yin, and Q. Peng, "Optimizing hybrid cooling strategy for enhanced thermal management of Lithium-ion battery packs at high discharge rates," *Applied Thermal Engineering*, vol. 295, p. 130611, May 2026, doi: 10.1016/j.applthermaleng.2026.130611.

[13] B. Suhendra, N. Alif Indratma, E. Kusrini, N. Putra, and M. Hasanuzzaman, "Thermal performance and temperature uniformity of battery modules using static single phase immersion cooling with multiple dielectric fluids," *Applied Thermal Engineering*, vol. 296, p. 130774, Jun. 2026, doi: 10.1016/j.applthermaleng.2026.130774.

[14] J. Kim, J. Oh, and H. Lee, "Review on battery thermal management system for electric vehicles," *Applied Thermal Engineering*, vol. 149, no. September 2018, pp. 192–212, 2019, doi: 10.1016/j.applthermaleng.2018.12.020.

[15] N. Bianco, A. Fragnito, M. Iasiello, V. Orlanducci, and F. Piccirillo, "Numerical evaluation of different cooling strategies for cylindrical battery packs: from air natural convection to topology-optimized cold plates," *International Journal of Thermal Sciences*, vol. 225, p. 110773, Jul. 2026, doi: 10.1016/j.ijthermalsci.2026.110773.

[16] S. Hekmat and G. R. Molaeimanesh, "Hybrid thermal management of a Li-ion battery module with phase change material and cooling water pipes: An experimental investigation," *Applied Thermal Engineering*, vol. 166, p. 114759, Feb. 2020, doi: 10.1016/j.applthermaleng.2019.114759.

[17] A. A. Pesaran, "Battery Thermal Management in EVs and HEVs: Issues and Solutions," in *Advanced Automotive Battery Conference*, 2001.

[18] C. Roe *et al.*, "Immersion cooling for lithium-ion batteries – A review," *Journal of Power Sources*, vol. 525, p. 231094, Mar. 2022, doi: 10.1016/j.jpowsour.2022.231094.

[19] A. S. Bidwaik, S. S. Bhusnoor, and S. R. Nikam, "Energy-optimized microchannel liquid cooling for 21700 lithium-ion battery packs," *Thermal Science and Engineering Progress*, vol. 73, p. 104638, May 2026, doi: 10.1016/j.tsep.2026.104638.

[20] A. Sharma, S. Sreedhara, M. Khatamifar, and W. Lin, "Comparative investigation of different liquid-cooled battery thermal management systems (LC-BTMS) designs for battery module of electric vehicle," *Applied Thermal Engineering*, vol. 292, p. 130436, Apr. 2026, doi: 10.1016/j.applthermaleng.2026.130436.

[21] J. Weng, D. Ouyang, X. Yang, M. Chen, G. Zhang, and J. Wang, "Optimization of the internal fin in a phase-change-material module for battery thermal management," *Applied Thermal Engineering*, vol. 167, p. 114698, Feb. 2020, doi: 10.1016/j.applthermaleng.2019.114698.

[22] X. Ding, Y. Wang, X. Yuan, D. A. Khan, J. Gu, and Z. Yang, "Design of cold plate structures for energy storage battery cooling and analysis of heat transfer performance," *Thermal Science and Engineering Progress*, vol. 72, p. 104612, Apr. 2026, doi: 10.1016/j.tsep.2026.104612.

[23] J. Smith, R. Singh, M. Hinterberger, and M. Mochizuki, "Battery thermal management system for electric vehicle using heat pipes," *International Journal of Thermal Sciences*, vol. 134, pp. 517–529, Dec. 2018, doi: 10.1016/j.ijthermalsci.2018.08.022.

[24] R. Sukarno *et al.*, "Innovative Pickup Car Cooling System Based on Thermoelectric Coupled With Heat Pipe Sink," *Automotive Experiences*, vol. 8, no. 2, pp. 296–309, Sep. 2025, doi: 10.31603/ae.13494.

[25] R. Sukarno, A. Premono, Y. Gunawan, A. Wiyono, and A. Lubi, "Experimental Investigation of Using Thermoelectric Coolers under Different Cooling Methods as An Alternative Air Conditioning System for Car Cabin," *Automotive Experiences*, vol. 7, no. 2, 2024, doi: 10.31603/ae.11485.

[26] M. F. Jauhari *et al.*, "Experimental Analysis of a Hybrid-Configured Battery Thermal Management System Using Paraffin Oil and Fan," *Automotive Experiences*, vol. 8, no. 3, pp. 612–623, 2025, doi: 10.31603/ae.13403.

[27] A. R. Abrari, T. H. Ariwibowo, D. Pramadihanto, N. R. Arini, E. H. Binugroho, and A. Miyara, "Thermal Performance Enhancement of Serpentine Cooling Design Using Branch Modification for Lithium-Ion Batteries," *Automotive Experiences*, vol. 7, no. 3, pp. 552–566, Dec. 2024, doi: 10.31603/ae.12709.

[28] N. T. Atmoko, A. Jamaldi, and T. W. B. Riyadi, "An Experimental Study of the TEG Performance using Cooling Systems of Waterblock and Heatsink-Fan," *Automotive Experiences*, vol. 5, no. 3, pp. 361–367, 2022, doi: 10.31603/ae.6250.

[29] W. Tong, K. Somasundaram, E. Birgersson, A. S. Mujumdar, and C. Yap, "Thermo-electrochemical model for forced convection air cooling of a lithium-ion battery module," *Applied Thermal Engineering*, vol. 99, pp. 672–682, Apr. 2016, doi: 10.1016/j.applthermaleng.2016.01.050.

[30] A. Kumar Thakur *et al.*, "A state-of-the art review on advancing battery thermal management systems for fast-charging," *Applied Thermal Engineering*, vol. 226, p. 120303, May 2023, doi: 10.1016/j.applthermaleng.2023.120303.

[31] L. Zhao, J. Wang, M. Zheng, and M. Chen, "Design and performance optimization of liquid immersion cooling system for prismatic lithium-ion battery modules," *International Journal of Heat and Fluid Flow*, vol. 118, p. 110181, Mar. 2026, doi: 10.1016/j.ijheatfluidflow.2025.110181.

[32] Z. Jiang *et al.*, "Immersion cooling battery thermal management system design and optimization for high-energy-density battery packs: A comparative study with side cooling plates," *International Journal of Heat and Mass Transfer*, vol. 261, p. 128550, Jun. 2026, doi: 10.1016/j.ijheatmasstransfer.2026.128550.

[33] L. Zhang *et al.*, "Post-venting immersion cooling of over-heated battery: Effect of thermal runaway risk, cell scale, and quenching strategy," *Process Safety and Environmental Protection*, vol. 210, p. 108730, Apr. 2026, doi: 10.1016/j.psep.2026.108730.

[34] Y. Lu, B. Sun, L. Li, F. Huang, and C. Chen, "Numerical investigation of vertical vibration effects on immersion cooling heat transfer for lithium-ion battery at high discharge rate," *Case Studies in Thermal Engineering*, vol. 77, p. 107607, Jan. 2026, doi: 10.1016/j.csite.2025.107607.

[35] C. Mo, A. C. Y. Yuen, Y. Wu, B. Fei, and J. Wang, "Experiments on the effects of immersion cooling on lithium-ion battery module and mitigating battery thermal runaway," *Journal of Energy Storage*, vol. 154, p. 121373, Apr. 2026, doi: 10.1016/j.est.2026.121373.

[36] M. A. Adit, S. Hasan, and N. N. Mustafi, "Performance analysis of a novel battery thermal management system integrating thermoelectric and dielectric immersion cooling in EVs," *Energy Conversion and Management: X*, vol. 30, p. 101550, May 2026, doi: 10.1016/j.ecmx.2026.101550.

[37] T. Ouyang, Z. Wang, G. Huang, Y. Li, and Z. Huang, "An integrated thermoelectric cooling design for preventing thermal runaway propagation in lithium-ion batteries," *Energy Conversion and Management*, vol. 356, p. 121327, May 2026, doi: 10.1016/j.enconman.2026.121327.

[38] S. K. Chung, Y. Jo, S. Baik, S.-W. Kang, and K. Choi, "Enhanced cooling performance of hybrid battery thermal management system with thermoelectric modules and multi-layered phase change materials," *Journal of Energy Storage*, vol. 155, p. 121587, Apr. 2026, doi: 10.1016/j.est.2026.121587.

[39] Z. M. Marouf, M. A. Fouad, and M. A. Hassan, "Experimental investigation of the effect of air bubbles injection on the performance of a plate heat exchanger," *Applied Thermal Engineering*, vol. 217, p. 119264, Nov. 2022, doi: 10.1016/j.applthermaleng.2022.119264.

[40] S. S. Hasan, A. Sh. Baqir, and H. B. Mahood, "The Effect of Injected Air Bubble Size on the Thermal Performance of a Vertical Shell and Helical Coiled Tube Heat Exchanger," *Energy Engineering*, vol. 118, no. 6, pp. 1595–1609, 2021, doi: 10.32604/EE.2021.017433.

[41] Z. M. Marouf and M. A. Fouad, "Combined Energetic and Exergetic Performance Analysis of Air Bubbles Injection into a Plate Heat Exchanger: An Experimental Study," *Energies*, vol. 16, no. 3, p. 1164, Jan. 2023, doi: 10.3390/en16031164.

[42] F. L. Rashid *et al.*, "An Examination of Air-Bubble Injection Mechanisms for Optimising Heat Transfer in Industrial Applications," *International Journal of Heat and Technology*, vol. 41, no. 5, pp. 1226–1248, Oct. 2023, doi: 10.18280/ijht.410513.

[43] H. Liu, C. Shi, C. Liu, and W. Chang, "A Review of Lithium-Ion Battery Thermal Management Based on Liquid Cooling and Its Evaluation Method," *Energies*, vol. 18, no. 17, p. 4569, Aug. 2025, doi: 10.3390/en18174569.

[44] M. U. Z. Priyadi *et al.*, "Systematic review of battery cooling technologies in electric vehicles: Methods, challenges, and recent innovations," *Mechanical Engineering for Society and Industry*, vol. 5, no. 2, pp. 434–458, Dec. 2025, doi: 10.31603/mesi.14070.

[45] I. G. N. B. Catrawedarma, S. Ton, D. D. Pranowo, and F. Surahmanto, "Hydrodynamic characteristics of the microbubble dissolution in water using an ejector-type bubble generator," *Case Studies in Chemical and Environmental Engineering*, vol. 11, p. 101043, Jun. 2025, doi: 10.1016/j.cscee.2024.101043.

[46] I. Catrawedarma, S. Ton, D. D. Pranowo, and F. Surahmanto, "Size Distribution and Mean Diameter of Microbubbles in Different Types of Ejector Bubble Generators," *Journal of Applied Fluid Mechanics*, vol. 18, no. 4, Jun. 2025, doi: 10.47176/jafm.18.6.3227.

[47] E. N. Sari, A. Fiveriati, N. Rusti, J. Rulianto, R. Bhiqman Susanto, and I. G. N. B. Catrawedarma, "Visual and Pressure Signal Investigations on Bubble Produced by Ejector Bubble Generator," *E3S Web of Conferences*, vol. 483, p. 03020, Jan. 2024, doi: 10.1051/e3sconf/202448303020.

[48] I. Catrawedarma, Deendarlianto, and Indarto, "Statistical Characterization of Flow Structure of Air–water Two-phase Flow in Airlift Pump–Bubble Generator System," *International Journal of Multiphase Flow*, vol. 138, p. 103596, May 2021, doi: 10.1016/j.ijmultiphaseflow.2021.103596.

[49] I. Catrawedarma, Deendarlianto, and Indarto, "Hydrodynamic behaviors of air–water two-phase flow during the water lifting in a bubble generator type of airlift pump system," *Heat and Mass Transfer*, vol. 58, no. 6, pp. 1005–1026, Jun. 2022, doi: 10.1007/s00231-021-03157-z.

[50] I. G. N. B. Catrawedarma, F. A. Resnaraditya, Deendarlianto, and Indarto, "Statistical characterization of the flow structure of air-water-solid particles three-phase flow in the airlift pump-bubble generator system," *Flow Measurement and Instrumentation*, vol. 82, p. 102062, Dec. 2021, doi: 10.1016/j.flowmeasinst.2021.102062.

[51] A. Adham, N. Mohd-Ghazali, and R. Ahmad, "Optimization of nanofluid-cooled microchannel heat sink," *Thermal Science*, vol. 20, no. 1, pp. 109–118, 2016, doi: 10.2298/TSCI130517163A.

[52] W. Wu, S. Wang, W. Wu, K. Chen, S. Hong, and Y. Lai, "A critical review of battery thermal performance and liquid based battery thermal management," *Energy Conversion and Management*, vol. 182, pp. 262–281, Feb. 2019, doi: 10.1016/j.enconman.2018.12.051.

[53] S. Pincus, "Approximate entropy (ApEn) as a complexity measure," *Chaos: An Interdisciplinary Journal of Nonlinear Science*, vol. 5, no. 1, pp. 110–117, Mar. 1995, doi: 10.1063/1.166092.

[54] A. Delgado-Bonal and A. Marshak, "Approximate Entropy and Sample Entropy: A Comprehensive Tutorial," *Entropy*, vol. 21, no. 6, p. 541, May 2019, doi: 10.3390/e21060541.

[55] S. Zurek, P. Guzik, S. Pawlak, M. Kosmider, and J. Piskorski, "On the relation between correlation dimension, approximate entropy and sample entropy parameters, and a fast algorithm for their calculation," *Physica A: Statistical Mechanics and its Applications*, vol. 391, no. 24, pp. 6601–6610, Dec. 2012, doi: 10.1016/j.physa.2012.07.003.

[56] P. Grassberger and I. Procaccia, "Estimation of the Kolmogorov entropy from a chaotic signal," *Physical Review A*, vol. 28, no. 4, pp. 2591–2593, Oct. 1983, doi: 10.1103/PhysRevA.28.2591.

[57] V. S. Anishchenko and S. Astakhov, "Relative kolmogorov entropy of a chaotic system in the presence of noise," *International Journal of Bifurcation and Chaos*, vol. 18, no. 09, pp. 2851–2855, Sep. 2008, doi: 10.1142/S021812740802210X.